Synthesis of 2D perovskite crystals via progressive transformation of quantum well thickness

Jin Hou, Wenbin Li, Hao Zhang, Siraj Sidhik, Jared Fletcher, Isaac Metcalf, Surendra B. Anantharaman, Xinting Shuai, Anamika Mishra, Jean-Christophe Blancon, et al.

Nature Synthesis; https://doi.org/10.1038/s44160-023-00422-3

Deterministic synthesis of phase-pure 2D perovskite crystals via progressive transformation of quantum well thickness

Jin Hou[1], Wenbin Li[2,3], Hao Zhang[2,3], Siraj Sidhik[1], Isaac Metcalf[1], Surendra B. Anantharaman[4], Xinting Shuai,[1] Anamika Mishra,[2] Jean-Christophe Blancon[2], Claudine Katan[5], Deep Jariwala[4], Jacky Even[6], Mercouri G. Kanatzidis[7] and Aditya D. Mohite[1,2*]

[1]Department of Materials Science and NanoEngineering, Rice University, Houston, Texas 77005, USA.

[2]Department of Chemical and Biomolecular Engineering, Rice University, Houston, Texas 77005, USA.

[3]Applied Physics Graduate Program, Smalley-Curl Institute, Rice University, Houston, TX, 77005, USA.

[4]Department of Electrical and Systems Engineering, University of Pennsylvania, Philadelphia, PA 19104, USA.

[5]Univ Rennes, ENSCR, INSA Rennes, CNRS, ISCR (Institut des Sciences Chimiques de Rennes) - UMR 6226, F-35000 Rennes, France.

[6]Univ Rennes, INSA Rennes, CNRS, Institut FOTON - UMR 6082, 35708 Rennes, France.

[7]Department of Chemistry and Department of Materials Science and Engineering, Northwestern University, Evanston, Illinois 60208, USA.

Two-dimensional (2D) multilayered halide perovskites have emerged as a platform for understanding organic-inorganic interactions, tuning quantum confinement effects and realizing efficient and durable optoelectronic devices. However, a major bottleneck has been reproducibly producing 2D perovskite crystals with desired perovskite-layer thicknesses (quantum well thickness, also known as n values) greater than two with the existing crystal growth methods. Here, we demonstrate a novel method termed kinetically controlled space confinement (KCSC) for the deterministic growth of phase pure Ruddlesden-Popper (RP) and Dion-Jacobson (DJ) 2D perovskites. The phase-pure growth is achieved by progressively increasing the temperature (for a fixed time) or the crystallization time (fixed temperature), which allows for acute control of the crystallization kinetics. In-situ photoluminescence spectroscopy and imaging suggest that the controlled increase in n-value (from lower to higher values of n=4, 5, and 6) occurs due to intercalation of excess precursor ions. Based on data from 250 experimental runs, phase diagrams for both RP and DJ perovskites have been constructed to predict the growth of 2D phases with specific n-values, facilitating the production of 2D perovskite crystals with desired layer thickness.

Two-dimensional halide perovskites (2D-HaP) have emerged as a new class of highly durable solution-processed organic-inorganic (hybrid) low-dimensional semiconductors.[1–3] They exhibit a unique combination of properties derived from four exciting classes of materials - quantum wells,[4] atomically thin 2D materials[5], organic semiconductors[6,7], and 3D-HaP perovskites[8,9]. The general chemical formula of 2D-HaP is $(A')_m(A)_{n-1}M_nX_{3n+1}$ (where A′ is a bulky organic cation, A is a small organic cation, M is a divalent metal, X is a halide, with m=2 in Ruddlesden-Popper (RP) phases and m=1 in Dion-Jacobson (DJ) phases, and n determines the thickness of the perovskite layer), which consists of alternate layers of organics $(A')_m$ and hybrid $(A)_{n-1}M_nX_{3n+1}$, providing a perfect platform to engineer hybrid composites with attractive optoelectronic properties . There is growing consensus that their physical properties are dictated by the interaction between the organic cation and the inorganic framework, which presents a unique opportunity to understand and tailor their behaviors,[10] including, charge-carrier mobility,[11,12] nonlinear optical effects,[13] tunable light emission,[14,15] electron-phonon coupling,[16] ferroelectricity,[17,18] Rashba effect[19] and transfer of chirality.[20] However, most of these studies on 2D HaPs have been performed on lower n-values (n=1, 2) largely due to difficulties in reproducibly growing higher n-value phase pure crystals and films (n>2) [5,13,21–23]. We hypothesize that the mixed phases (multiple n-values) largely arise from the lack of sufficient control of crystallization kinetics (temperature, time) using the classical synthesis (CS) method for the growth of 2D HaP crystals and powders. Briefly, the CS method used across the perovskite research community involves dissolving all precursors in a solvent at an elevated temperature (230 °C) to achieve a supersaturated solution, followed by rapid crystallization through fast cooling by removing the solution from the hot plate to the ambient.[1–3,24] Once the temperature reaches below a certain point where supersaturation is excessive, nucleation will dominate, which results in a large number of small crystals (a few micrometers in size) in a short period of time (5-10 minutes). The fast nucleation due to the fast-cooling (230 °C to 25 °C almost instantaneously) makes it challenging to control the rate of crystallization and can result in the heterogeneous growth of unwanted phases. Therefore, we hypothesize that decoupling the crystallization temperature and time would enable a much better control over the kinetics of growth, which is challenging to achieve using the CS method since there is limited freedom to control the temperature or time one at a time during the crystallization process. As a result, understanding the impact of the kinetic parameters on realizing phase pure 2D perovskites has been largely unexplored and systematic studies on the effect on tuning the temperature or time of

crystallization for a given stoichiometry are still missing. In addition to difficulties in achieving phase pure crystals using the CS method, the powder forms of 2D-HaP are limited by their small crystal sizes (μm to mm sizes), making it challenging to precisely analyze the intrinsic physical properties such as (i) Light-matter interactions;[25–27] (ii) Optical measurement and dielectric functions where large-area flat crystals are required;[4] (iii) Electron-phonon interactions, where carrier trapping and exciton dissociation at grain boundaries or edges can often lead to complicated spectra.[28–30]

Attempts to cultivate large 2D hybrid perovskite (HaP) crystals have been made by slowing down growth through increased crystallization temperature and dilution,[31,32] but with limited success in achieving higher n-values ($n \geq 4$).[1,24,30,33–35] Hence, the traditional methods of acquiring high n-value crystals have involved either (i) separating n-pure crystallites from an n-mixed crystal[24] or (ii) making several synthesis attempts. Nonetheless, a direct and reliable technique for producing phase-pure high n-value crystals is imperative.

Here we demonstrate that by either prolonging the crystallization time at a constant temperature or adjusting the synthesis temperature at a constant crystallization time, the initial 2D-HaP crystal can transform from lower to higher n-values. This transformation was verified through in-situ absorbance and x-ray diffraction measurements. To control the crystallization kinetics, we confined the precursor solution's volume between two glass slides and mounted it on a hot plate to precisely regulate the heating and cooling rates. In-situ photoluminescence spectroscopy and imaging suggest that the transformation from a lower n-value to a higher n-value starts from the edges of the preformed crystals, eventually converting the entire crystal into higher-n 2D-HaP crystals. Based on the experimental data collected from the KCSC method, we created multi-parameter phase diagrams for both the RP and DJ 2D-HaP using machine learning. Finally, we show that the concept of isothermal control can be translated to the CS process used commonly across the research community to synthesize powders of 2D-HaP, which allows us to synthesize 2D-HaPs from n=1-6. We believe that the direct and reproducible approach method we propose for obtaining phase-pure single crystals and powders can be applied to RP and DJ-based perovskites of varying compositions. This will allow for a broader investigation of the physical properties of these perovskites, which has been previously limited to those with n=1 or 2.

Furthermore, these studies may uncover new opportunities for technological applications beyond using these perovskites solely as passivation layers or additives in bulk 3D perovskite films.[33,36]

1. Result and discussion

1.1 KCSC method and transformation

The progressive transformation to high n is demonstrated via the KCSC method, which is illustrated in Fig. 1a. To observe the transformation phenomenon, we used a parent solution of low n-value (n=3) stoichiometry (mol ratio, Pb: MA: BA=4: 2.67: 1.71) of $BA_2MA_{n-1}Pb_nI_{3n+1}$ to obtain large-area crystals of high n-values (n=4-6) by tuning the crystallization temperature and time. First, same as in CS, all the precursors (PbO, Methylammonium chloride (MACl), and Butylamine (BA)) are dissolved and mixed in the hydroiodic acid with the concentration of 0.85 M (based on Pb) at 190 ◦C. To prevent supersaturation and promote gradual growth of crystals, the solution is diluted by a factor of two. The diluted solution is then sandwiched between two preheated glass substrates treated with UV-ozone and placed on a hotplate for annealing at varying temperatures. When the substrate is annealed between 55°C and 105°C, a large crystal grows gradually due to limited solvent evaporation at the substrate's edge. Annealing below 55°C or above 105°C is not recommended as evaporation is minimal or the solution boils off, respectively. At a relatively low temperature within this range, the resulting crystal's n value corresponds to the parent solution's stoichiometry. For instance, annealing a parent solution of RP with n=3 stoichiometry below 76°C produces a crystal with an n value of 3. Conversely, annealing at a higher temperature between 80°C and 105°C leads to the formation of higher n values such as n=4 and 5 as the initial crystal. If the temperature is kept constant and the crystal is monitored over time, the initial n value will transform into higher n values, regardless of the starting n-value.

We performed in-situ optical absorbance and X-ray spectroscopy measurements on the RP 2D-HaP crystal fabricated by the KCSC method using a parent solution with the stoichiometry of n=3, where we tuned the temperature and time separately. For the time-dependent experiment, we increased the time of crystallization at a fixed temperature. For the temperature-dependent experiment, we varied the temperature of synthesis for a fixed crystallization time. Figure 1b illustrates the evolution of optical absorption as a function of temperature (ranging from 60-100 ◦C) for a fixed time of 7 hours using the same n=3 stoichiometry parent solution. At low temperatures

(60-66 °C), we observed the formation of the n=3 crystal, which was identified based on the exciton absorption peak at 2.04 eV and also validated by comparison with that of the n=3 single crystal.[1,4] However, as we increase the temperature further to 68-79 °C, we observe a new peak at 1.92 eV, which is redshifted from the n=3 peak. When further increasing the temperature from 80 °C to 100 °C, we observed yet another set of peaks emerge at 1.85 eV and 1.8 eV. Evaluation of the peak positions and their comparison with a single crystal of 2D-HaP fabricated using the classical method suggests that these peaks at 1.92 eV, 1.85 eV, and 1.8 eV corresponding to n=4, n=5, and n=6 respectively,[1,4] which were further validated using x-ray diffraction measurements as shown in Fig. 1c. Briefly, the n=3 crystal is formed at 60 °C indicated by the set of corresponding (0*k*0) peaks consistent with the n=3 single crystals previously synthesized[1,4,24] , which upon increasing the temperature to 80 °C, gives rise to (0*k*0) peaks of n=4 with a concomitant decrease in the intensity of the n=3 peaks. As we further increased the temperature to 100 °C, (0*k*0) peaks of n=5 appeared and dominated, with the decreasing of the n=4 peaks. The evolution from n=3 to n=4 and finally n=5 observed in x-ray diffraction measurements is consistent with the temperature-dependent absorption measurements.

We changed the duration of crystallization at a constant temperature of 75°C and monitored the growth of a single perovskite crystal after every one-hour interval. The absorbance spectra versus time for the KCSC method are displayed in Figure 1d. Initially, n=3 was formed within 4 hours, followed by n=4 after 5 hours, causing the original n=3 excitonic peak intensity to decrease. Heating the crystal further at 75°C resulted in its transformation to n=5 after 13 hours. However, the crystal did not quickly convert from n=5 upon continued annealing, which is expected since the n=6 compound is less thermodynamically favorable.[24] The optical absorbance measurements are further supported by time-dependent XRD measurement as shown in Fig. 1e, and Fig. S1, where a n=3 crystal slowly transforms to n=4 after 7 hours of growth and finally to n=5 after 13 hours. These measurements clearly show that we can tune the n value progressively by controlling temp and time separately.

The lateral size of the crystal fabricated by the KCSC method is a few millimeters to centimeters depending on the growth time. The thickness of the crystals is around 500 nm, which was calibrated to the amount of solution (Fig. S2) and the top glass slide used to confine the solution

since the spacing between two substrates could be tuned by varying the pressure applied to the apparatus.[31] XRD measurements suggest that the orientation of the crystals are along the stacking

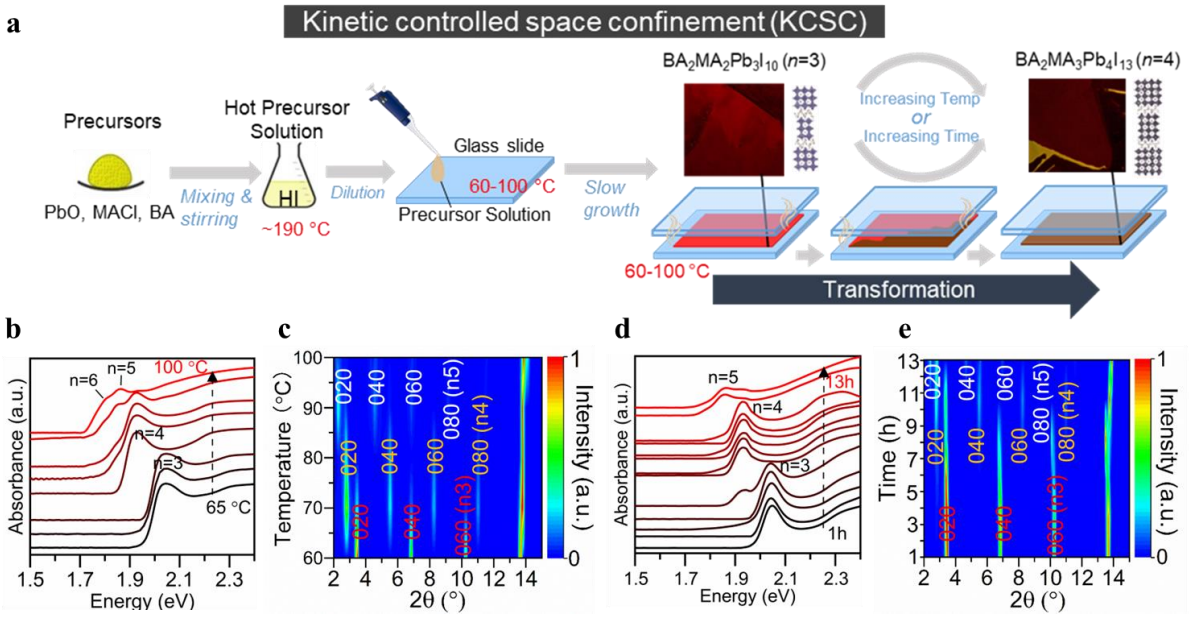

Fig. 1 | Transformation of 2D RPPs (*n*=3) in KCSC. (**a**) Schematic illustration of the kinetically controlled space confinement method (KCSC) to grow large area crystals with high n-value via progressive transformation. (**b**) In-situ absorbance and (**c**) 1D X-Ray spectrum as a function of the crystallization temperature. (**d**) In-situ absorbance and (**e**) 1D X-Ray spectrum as a function of the crystallization time.

axis (or in-plane) as determined from the characteristic low angle (0k0) reflections corresponding to the lattice constants in the stacking direction (Figure S3) with no detectable signal of (111) perovskite peak. Experimental Grazing incident wide-angle X-ray (GIWAX) measurements (Fig. S4) match with simulated indexing of horizontally oriented 2D perovskite structure, indicating the in-plane orientation of the perovskite layers.[36]

To rationalize the transformation in 2D HaP from a thermodynamics perspective, we calculate the enthalpy of formation (ΔH) and the Gibbs free energy (ΔG) for the RP 2D-HaP crystal. The enthalpy of transformation was calculated based on the reaction scheme given in table S1, where the reactants are a specific n-value crystal, PbI_2, MACl while the product is the (n+1) number crystal (Fig. S5, Table S3-S5). Since $\Delta G = \Delta H - T(\Delta S)$, for the temperature-dependent transformation, we have that ΔG is mainly dependent on the ΔH since the change of entropy ΔS is negligible[24]. The negative ΔH value of -62.5 KJ/mol for the n=3 to n=4 transformation indicates it is favorable. For the transformation of n=4 to n=5, the ΔH becomes more positive indicating a

low probability of fabricating a phase pure 2D perovskite. Furthermore, the transformation from n=5 to n=6 is extremely unfavorable because of the high enthalpy of transformation, equaling 149 KJ/mol (Table S3). To overcome the large energy barrier, parent solutions of higher n-values (n=4,5) were also tested with annealing at high temperature and long time. Higher n-value parent solutions facilitate the formation of higher n-value crystals compared to a n=3 solution, but with decreasing reproducibility. For a n=4 solution, a n=4 crystal is formed at low temperature (below 76 °C), while at very high temperature (105 °C) with long annealing time (10 hours) it can form n=6 crystal (Fig. S6). For parent solution of n≥5, a specific n-value can not be obtained and 3D HaP is formed instead since it is more thermodynamically favorable than higher n-value (ΔH_f: n=5 < MAPbI3(3D) < n=6).[24]

1.2 Building a multiparameter phase diagram

To get a global view of the transformations and the relationship between phase purity, temperature and time, we designed and performed over 250 KCSC temperature and time-dependent syntheses for both RP and DJ. For DJ syntheses, we chose 3AMP as the organic cation spacer and used the same experimental methodology as used for RP as illustrated in Fig. 2a. Our approach consisted of four steps: (i) synthesizing the crystal using the same parent solution but with varying temperature and time; (ii) performing large area optical absorption measurements on the crystal, analyzing the excitonic absorption peak position to determine the n-value and; (iii) mapping the resulting n-value as the function of the temperature and time parameters; (iv) deploying machine learning (ML) analysis to refine the map and produce the phase diagram with smooth boundaries. Fig. 2b shows the results of the experiment of 2D-HaPs using n=3 stoichiometry parent solution, each data point represents one synthesis performed at a specific temperature during a given time. We classified them into four categories: the purple points indicate n-mixed phases, the pink data points indicate n=3, orange indicates n=4, and yellow for n=5. The n-mixed phases are defined if the crystal contains more than one n value indicated by the multiple excitonic absorption peaks. However, we find that in some regions there is a large variance of the phase pure and mixed-phase crystals. For example, when synthesizing large area n=3 KCSC crystals at 70 °C and >8 hours, the border between phase pure and mixed phases is blurred. Our

results show that at 70 °C and 9 hours, the KCSC synthesis produces a mixed phase (Fig. 2b). However, at the same temperature but 10 hours, the sample is phase-pure n=3. To alleviate the uncertainty in these boundaries, we used supervised machine learning (ML) to statistically classify regions of pure phase vs mixed phase and to formulate a phase diagram (Fig. 2c). Specifically, we deployed a support vector machine classifier to find the most optimal hyperplane, which can separate the 2 classes, for this example n=3 and the mixed phase. Details of the ML method can be found in SI section 1.2.

For the RP type (Fig.2b), the crystals are phase-pure n=3 irrespective of the annealing time below 60 °C. As we slightly increase temperature (65 °C) the synthesized crystal at short annealing times are still phase pure, but at longer annealing times the crystal becomes a mixture of phases (n=3 and n=4). This indicates a fixed temperature higher than 65 °C is needed to trigger the transformation. At a fixed temperature of 77 °C, the phase diagram shows that at all times the KCSC method produces mixed phases. From 78 °C to 92 °C, the KCSC method produced phase

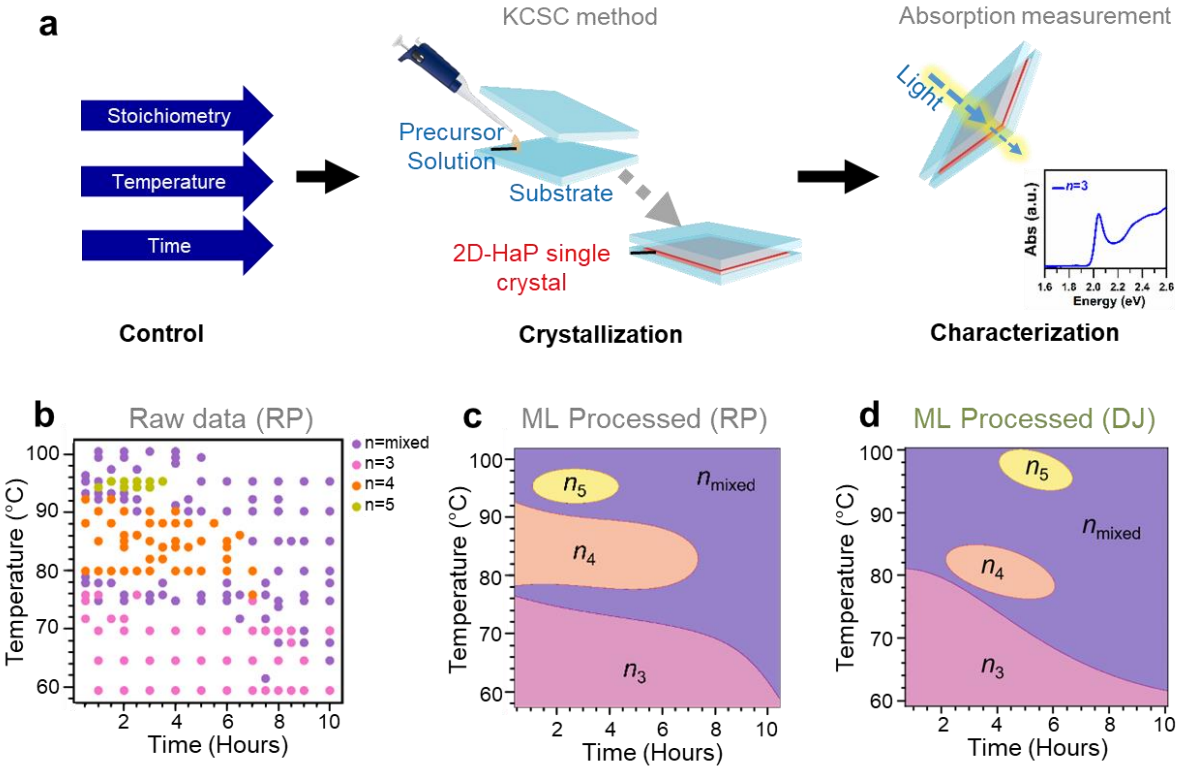

Fig. 2 | Refined phase diagram of n-purity and temperature, time of 2D HaP using KCSC method (**a**) Schematic illustration of the experimental methodology. (**b**) Resulting n-value (raw experimental data) as the function of the crystallization temperature and time. (**c**), (**d**) Refined phase diagram after classifying regions of different n using supervised machine learning for RP 2D-HaP and DJ 2D-Hap.

pure n =4 RP 2D-HaP right from the start of the annealing, which indicates that higher temperature will facilitate the formation of a higher n-value crystal, which is consistent with our thermodynamics calculations. As we increase the annealing time, the pure n=4 crystal also transforms into an n-mixed crystal because of intercalation. The pure n=5 crystal was acquired from a few conditions at higher temperatures (95 °C) but a relatively short time window. The phase diagram indicates that the temperature for isothermal transformations, determines the initial n-value and time controls the rate of the transformation.

Next, we investigate the DJ 2D-HaP using the same approach. As shown in fig. 2c, an ML-assisted mapping of crystals yielded by the KCSC method using 3-(aminomethyl) piperidinium (3AMP) DJ n=3 solution is plotted. By tuning the temperature and time of crystallization, the same parent n=3 solution formed crystals from n=3 to n=5 with high purity. The mapping of DJ 2D-HaP shows a similar trend compared to RP 2D-HaP, where the n-value increases as temperature and time of crystallization increase. The chances of synthesizing phase-pure crystal decrease with increasing n-value, which is demonstrated by the area decrease of the region area of ascendant-n in the map. Nonetheless, one difference between the RP and DJ phase diagram is: For DJ perovskites, the formation of higher n-values (n=4 and n=5) requires higher temperatures and longer times. This is attributed to the smaller interlayer spacing of DJ and additional interlayer interaction, limiting the precursor diffusion or the proposed intercalation mechanism (vide infra).[2,27,37] In summary, the concept of isothermal control demonstrated for both RP and DJ 2D-HaP series suggests it is generally applicable to all the 2D-HaPs.

1.3 Mechanism of transformation

To understand how the 2D-HaPs transform, we considered several possible pathways. Firstly, we looked at the concentration of the precursor solution and whether the loss of certain organic cations (Butyl Ammonium or aminomethyl pyridinium) during growth at high temperature could cause a change in concentration and thus a change in n value. Secondly, we examined whether the dissolution of lower n-value crystals and recrystallization of higher n-value crystals could contribute to the transformation. Thirdly, we considered the possibility that larger A' cations (such as BA) could escape from the perovskite structure during the transformation from n=3 to n=4-6. Finally, we looked at the idea that intercalation of MA^+, Pb^{2+}, and I^- from the crystal edges of the first formed 2D-HaP crystal could increase the perovskite-layer thickness. Initially, we explored

the possibility that the change in n value was due to the loss of organic spacer cations during the annealing process, which could alter the proportion of inorganic and organic components and thus change the stoichiometry to form higher n-values. To test this hypothesis, we conducted experiments on RP and DJ perovskites, which contain BA and AMP cations. The BA has a boiling point of 78 °C but AMP is at ~230 °C, which is much higher than our experimental temperature range (60 – 100 °C). The organic spacer would not likely escape faster than other cations (MA^+, Pb^{2+}, and I^-) from the solution, therefore we ruled out this possibility.

To test the second, third, and fourth potential-pathways, we set up an in-situ photoluminescence (PL) imaging and PL spectrum during the crystal growth process to visualize the transformation (Fig.3). The PL setup is shown in Fig. 3a, where we measured the emission of the 2D-HaP crystal by exciting the whole region using a mercury vapor lamp with a 532 nm short pass filter mount before the sample. This allowed us to photoexcite and image the photoluminescence from the crystal and collect spectrally resolved information during the transformation from low n to high n value. The PL images were collected by adding a Semrock Razoredge 633nm long pass filter right before the CCD camera. The filter suppresses the emission from the RP n=3 perovskite and allows for the detection of the n=4 phase. Figure 3c (Fig. S7) illustrates the evolution of the 2D-HaP single crystal as a function of time at 77 ◦C, the dark red region is n=3 and the brighter red region is n=4. After the n=3 crystal forms, under continuous heating we observe the appearance of the n=4 at the edge of the n=3 crystal, and then with time, the n=4 area expands and gradually converts the whole n=3 region to n=4. Simultaneously, we also probed the photoluminescence spectra as a function of the growth time as shown in Fig. 3b. The circle illustrated on the PL images (fig. 3c) is the probe region with a laser beam diameter of ~15 μm under a 10x objective. The spectra show a progressive change in emission peak from 630 nm to 650 nm indicating an increase in layer thickness from n=3 to n=4 which agrees with our hypothesis. In addition, the photoluminescence spectra show no other emissions from different sites, which excludes the possibility of defects and third-phase impurities. Lastly, both PL imaging and PL spectra results indicate that the transformation occurs much faster at the edges than in the bulk. We also probed the PL spectra from the back side of the crystal and the identical n was observed (fig.3d), which excluded the possibility that transformation is from a high n-value crystal forming on top of a lower n-value to form vertically stacked heterostructures.

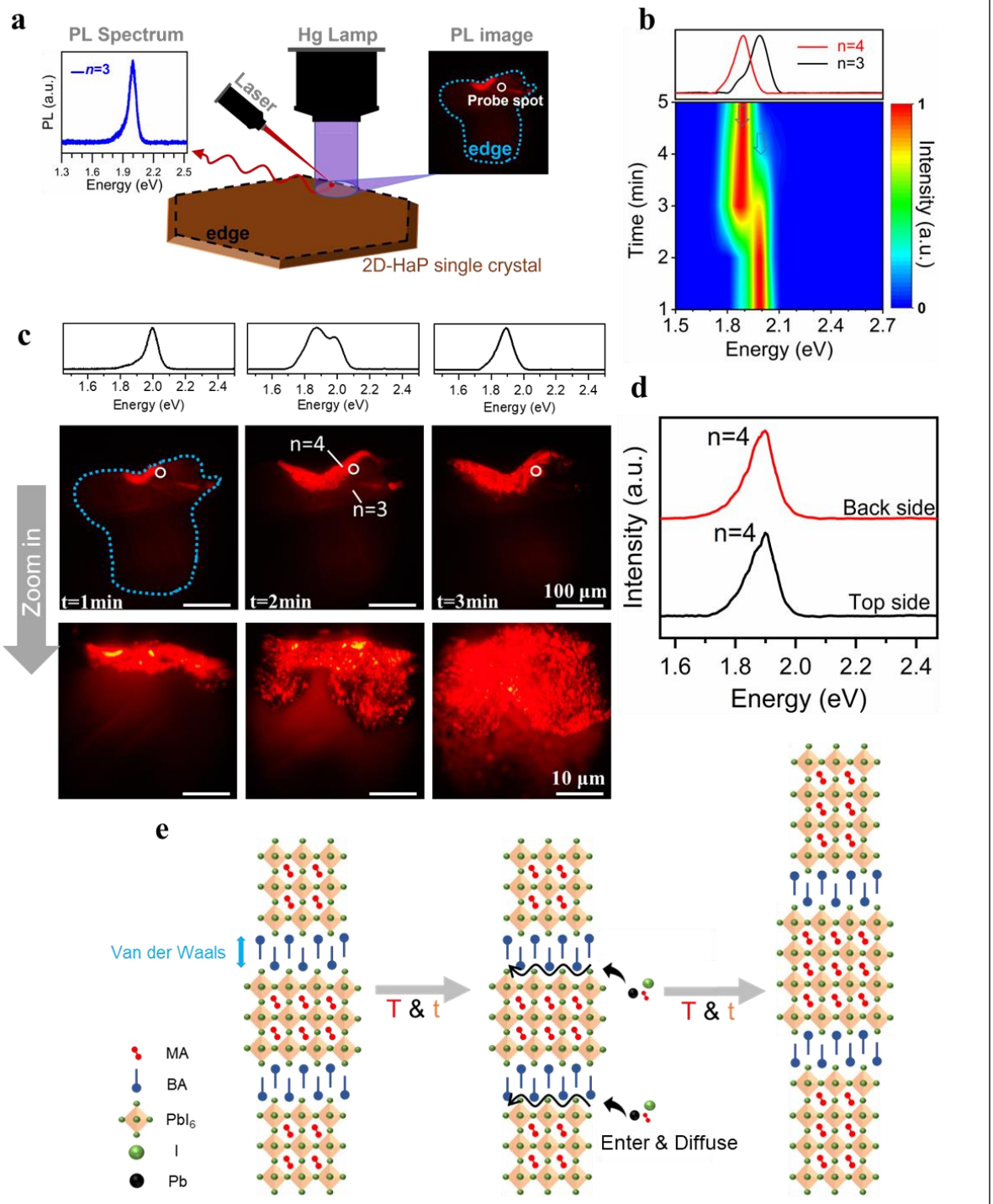

Fig. 3 | Mechanism of transformation of 2D RPPs (*n*=3) in KCSC. (**a**) Schematic illustration of In-situ PL imaging and spectrum set-up. (**b**) PL spectrum intensity evolution probed at white circled spots showed in fig (c) middle row. **(c)** In-situ time dependent PL imaging (middle row) depicting the transformation from n=3 to n=4 single crystal over 3 minutes. The dotted blue line shows the boundary of the formed crystal. The zoomed in version of the image is presented below. Top row shows the evolution of the PL spectrum for the corresponding PL images measured at spots specified by the white circle (circle size is not-to-scale). (**d**) Plot showing the PL measured from the back, and the front side of the crystal grown on a glass substrate. (**e**) Schematic of proposed intercalation mechanism.

Therefore, the second mechanistic hypothesis is also excluded since the transformation occurs without dissolving the n=3 and recrystallization of n=4. The third hypothesis was excluded after comparing our observations with a previous report by Fang et al,[38] wherein a PL quenching (PL intensity decay) occurred after the 2-phenyl ethyl ammonium (another organic cation forming RP 2D-HaP) left the perovskite framework due to laser-induced degradation. However, this is not the case observed in our PL experiments discussed in fig.3, where emissions from higher n emerged without a decrease in PL intensity.

Finally, we propose that the transformation is through an intercalation process, where small precursor ions, such as MA^+, Pb^{2+}, and I^- penetrate the lattice from the edges of the 2D-HaP crystal and diffuse along the interface between the perovskite layers. These ions fill the voids of the corner-sharing PbI_6 structure, forming additional linkages and integrate with the $[Pb_nI_{3n+1}]$ lattice. This templating effect occurs because of the weak ionic interactions between the 2D inorganic octahedral sheets and the organic spacers. Figure 3e illustrates the proposed intercalation growth mechanism for the RP-HaP. Here, in the solution, the n=3 perovskite forms first, which are shown by the stacking of 3 inorganic $[Pb_nI_{3n+1}]^{(n+1)-}$ layers separated by the butylammonium organic spacer cations. Then over time, the organic MA, Pb, and I molecules diffuse through the edges of the n=3 2D-HaP crystal and attach to the $[Pb_nI_{3n+1}]$ structure. The intercalation process results in the increase of the layer thickness from n=3 to n=4 for the synthesized 2D-HaP. This mechanism also explains the observation that DJ HaP requires higher temperature and longer time for transformation because of the extra H-bond between spacer cation and octahedral in DJ HaP, slowing down the intercalation. Our results are consistent with previous reports that observe the intercalation of precursor ions into the lattice to form 2D-HaP and higher layer thickness 2D-HaP. For e. g., Guo et al.[39] proposed that extra halide additives (K^+) would facilitate the intercalation of $PbBr_6^{4-}$ octahedra into the lower-n $PEA_2FA_{n-1}Pb_nBr_{3n+1}$ (PEA = phenylethylamine, FA = formamidine) to transform to higher n which is associated with Coulomb interaction.

1.4 Applying the KCSC to the classical method for batch-scale synthesis of 2D-HaPs powders

While the KCSC method provides excellent control over phase pure, large area high n-value (n=1-6) monocrystals of 2D-HaP, it is not scalable. As a result, with the goal of using the crystal transformation principle to achieve phase pure crystals in large quantities, we investigated the effects of controlling the temperature and time using a modified classical synthesis (CS) approach.

Figure 4a illustrates the CS method process, in which all the precursors are mixed in a concentrated hydriodic acid (HI) at a specific stoichiometric ratio according to the target n-value. The solution is heated to boiling and rapidly cooled to room temperature within 1 hour or even shorter period.

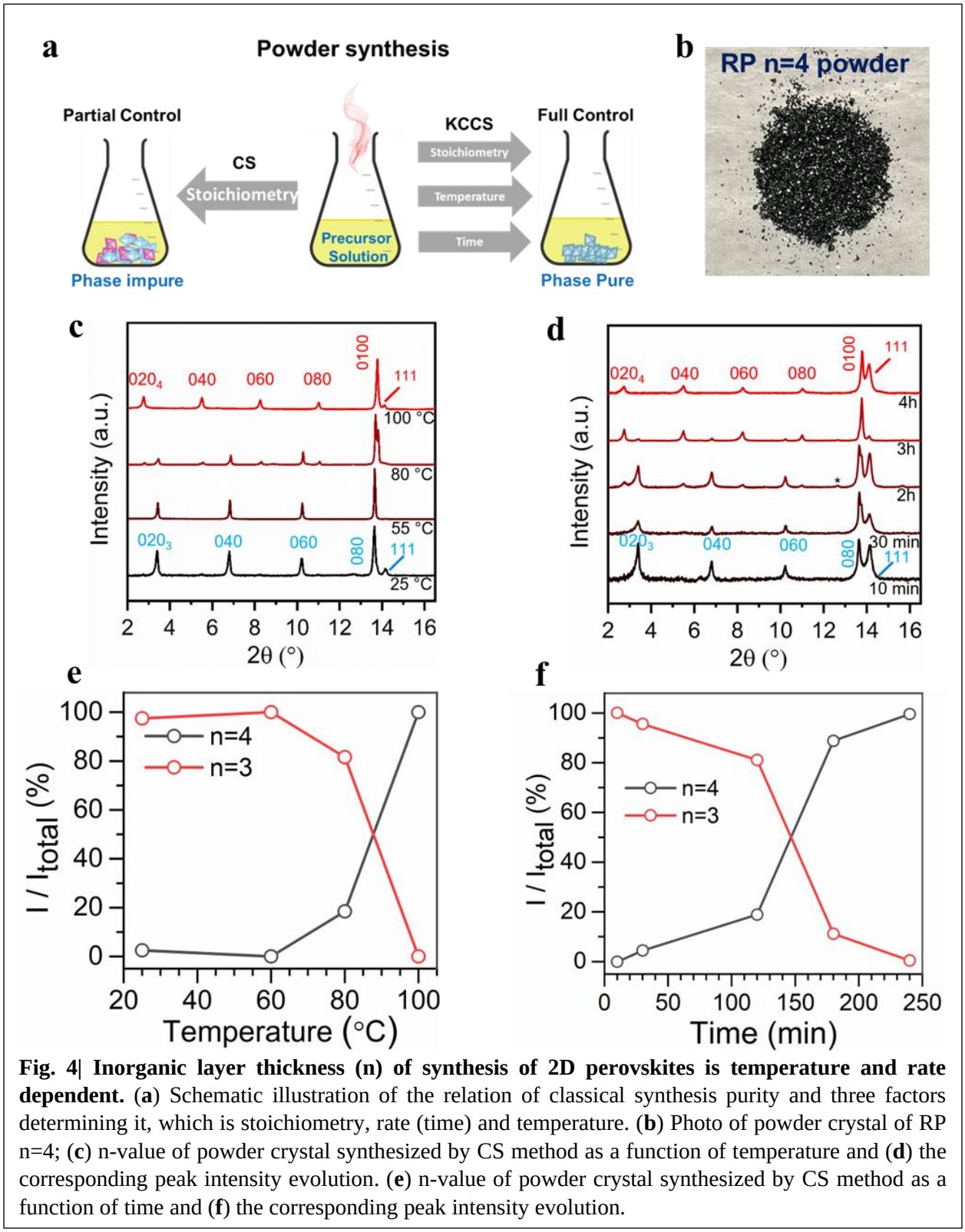

Fig. 4| Inorganic layer thickness (n) of synthesis of 2D perovskites is temperature and rate dependent. (**a**) Schematic illustration of the relation of classical synthesis purity and three factors determining it, which is stoichiometry, rate (time) and temperature. (**b**) Photo of powder crystal of RP n=4; (**c**) n-value of powder crystal synthesized by CS method as a function of temperature and (**d**) the corresponding peak intensity evolution. (**e**) n-value of powder crystal synthesized by CS method as a function of time and (**f**) the corresponding peak intensity evolution.

Small flakes with a typical lateral size of around 100 μm were obtained. However, polycrystalline samples produced from this CS method often contain mixtures of different n-values. For example, Fig. S8a shows the X-ray diffraction pattern for 10 classically synthesized n=3 RP samples, in which only 7 of the 10 syntheses achieved were phase-pure. The diffraction patterns of the unsuccessful synthesis show a consistent mixture of n=3 and n=4 phase (RP). Then we transposed the methodology developed in section 1.3 to the CS method. To ensure a uniform temperature across the precursor solution and also a prolonged cooling period, we immersed the reaction vial into an oil bath. The first parameter to tune is the temperature at which the boiling solution is left to crystallize. Instead of room temperature, we test a series of isothermal transformations, figure 4c shows the powder X-ray diffraction of 2D-HaP powder crystals synthesized from 25 °C to 100 °C. It shows a similar temperature dependent trend as observed in the KCSC method. Below 60 °C the n=3 forms but as the temperature is increased, the resulting powder becomes n=3 and n=4 mixture at around 80 °C and finally pure n=4 at 100°C. However, as we showed in Fig. S8, compared to room temperature, crystallization at 55 °C has a higher probability to obtain pure crystal, which is consistent with the previous discussion in which fast precipitation of the 2D perovskite crystals results in mixed phases.[40] Our findings suggest that a temperature range of 40-55 °C is essential for the consistent and pure production of 2D-HaP. Within this range, we are able to slow down the crystallization process without inducing any changes caused by higher temperatures. This highlights that the temperature at which the solution is cooled is just as important as stoichiometry in the traditional synthesis method. Next, we also explored the impact of varying the total duration of the crystallization process. Figure 4d illustrates the X-ray diffraction patterns for various crystallization times with the temperature set to 90 °C. The results show a trend similar to the KCSC in which, as the time increases, the crystal transitions from n=3 into a mixture of n=3 and n=4 and finally phase pure n=4 after 4 hours. Figure 4e and 4f are the intensity changes of the corresponding temperature and time-dependent XRD patterns, both of them show that n=3 completely converts to n=4. The temperature and time-dependent observations we have made clearly demonstrate that stoichiometry is not the sole determinant of the n-value in powder 2D-HaP. Precise control over all three parameters is crucial for the production of a single n-value 2D-HaP. As a result, we propose a new synthesis method called Kinetics-controlled classic synthesis (KCCS) that emphasizes the importance of the control of these parameters in powder synthesis.

1.5 Phase pure n=1 to n=6 of RP and DJ 2D-HaPs

Having established the importance of progressive transformation, we are able to grow phase pure single crystals ranging from n=1 to n=6 for both RP and DJ 2D-HaP. Figure 5a, 5b shows the absorption, and photoluminescence spectrum of KCSC produced n=1 to n=6 RP 2D-HaP single crystal. Each of the KCSC fabricated crystals exhibit a single narrow absorption peak decreasing from 2.42eV to 1.78eV as a function of n value (n=6 to n=1). The photoluminescence emission peak also follows this trend from 2.38eV to 1.77eV. This behavior is consistent with their quantum and dielectric confinement effects[41] and furthermore, indicates the phase purity of the fabricated crystals[4]. Both absorption and PL indicate the high purity of the crystal synthesized by our method. The absorption and photoluminescence of a control $MAPbI_3$ 3D-HaP are shown in the black curve

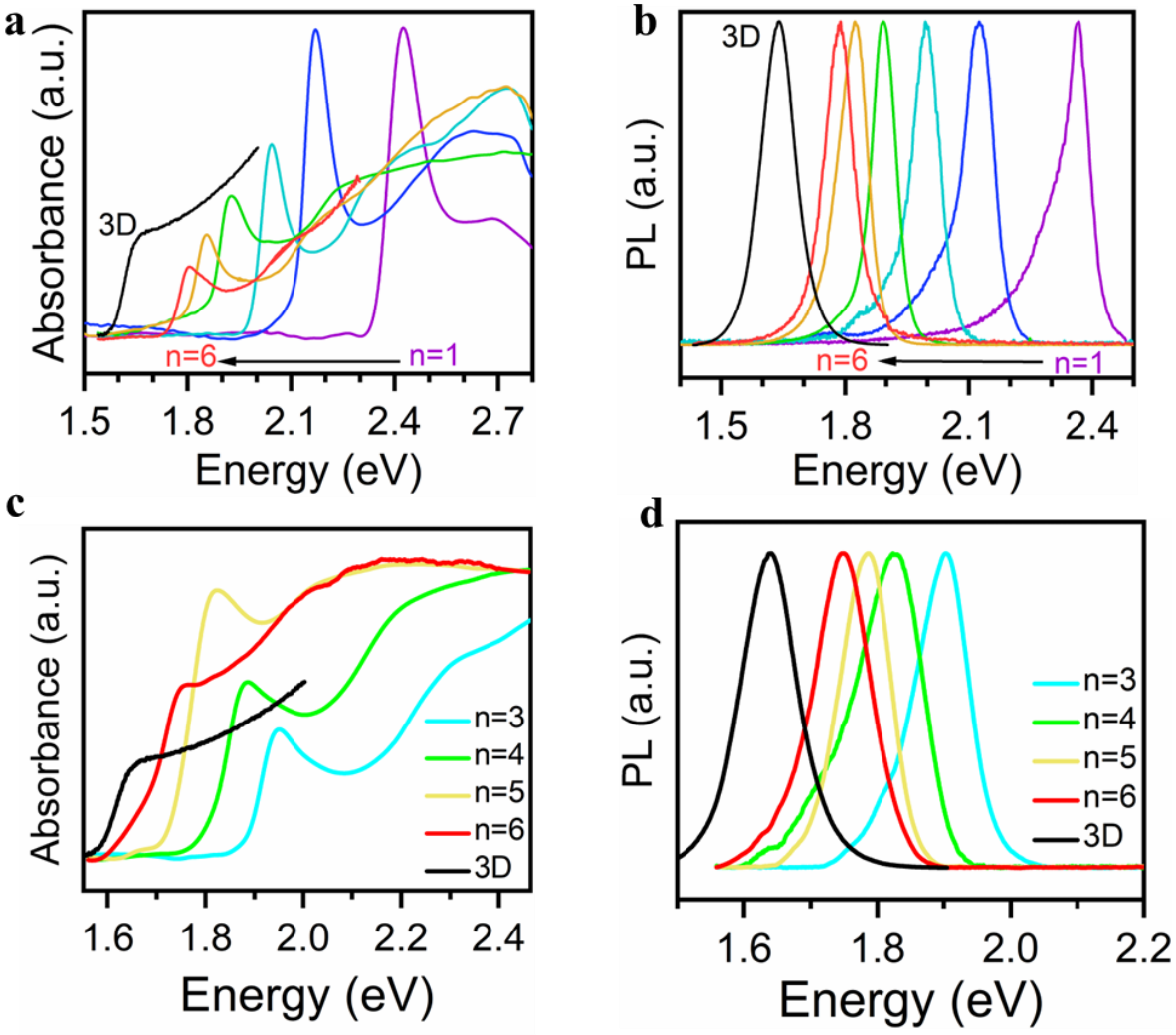

Fig. 5 | Synthesis capability of transformation based KCSC. (**a**) Absorbance, (**b**) PL of RP n=1 to n=6 and 3D $MAPbI_3$. (**c**) Absorbance, (**d**) PL of DJ n=3 to n=6 and 3D $MAPbI_3$.

on both plots. X-Ray diffraction of KCSC fabricated crystal (Fig. S9) also shows high purity. Figure 5c, d shows the absorption, and photoluminescence spectrum of KCSC produced n=3 to n=6 DJ 2D-HaP single crystal. Absorption (fig.5c) shows the 3AMP follows the general trend for 2D-HaP where the band gap decreases as n increases (1.95eV for n=3, 1.88eV for n=4, 1.82eV for n=5, 1.75eV for n=6). Steady-state photoluminescence (PL) shows an identical trend with the band gaps (1.90eV for n=3, 1.82eV for n=4, 1.79eV for n=5, 1.75eV for n=6). Similar to the 2D-HaP synthesized from KCSC and transformation, the DJ 2D-HaP synthesized by the same approach is of high purity. The band gap of the DJ 3AMP series is smaller than the RP BA series, consistent with previous reports.[2,37,42] Transformation of the 4-(aminomethyl)piperidinium (4AMP) 2D-HaP is shown in Fig. S10.

2. Methods

2.1 Crystal synthesis

2.1.1 Reagents: PbO (99.9%), Methylammonium chloride (MACl, 99.0%), Butylamine (BA, 99.0%), 4-(aminomethyl)piperidine (4AMP, 96%), hydroiodic acid (HI, 57 wt % in H2O, distilled, stabilized, 99.95%), hypophosphorous acid solution (H_3PO_2, 50 wt % in H2O) and diethyl ether ($(C_2H_5)_2O$, 98%, contains 2% ethanol and ~10ppm BHT) were purchased from Sigma-Aldrich. 3-(aminomethyl)piperidine (3AMP, 98%) was purchased from TCI, Methylammonium iodide (MAI) were purchased from Greatcellsolar. All chemicals were used as received.

2.1.2 Synthesis of $(BA)_2(MA)_{n-1}Pb_nI_{3n+1}$ KCSC parent solution and powder crystal: RP perovskites solution were synthesized by modifying the previously reported procedure[1]. For n = 1, PbO powder (892.8 mg, 4mmol) was dissolved in a mixture of 57% w/w aqueous HI solution (4.0 mL, 30.4 mmol) and 50% aqueous H_3PO_2 (1.0 mL, 9.1 mmol) at room temperature (25 °C) under constant magnetic stirring for 10 mins, which formed a bright yellow solution. In a separate beaker, n-$CH_3(CH_2)_3NH_2$ (369.6 μL, 4 mmol) was neutralized with HI 57% w/w (2 mL, 15.2 mmol) in an ice bath resulting in a clear yellow solution. The addition of the n-$CH_3(CH_2)_3NH_3I$ solution to the PbI_2 solution initially produced orange precipitates, which were slowly dissolved under heating the combined solution to boiling. The solution was then diluted 3 times by aqueous HI solution. For higher n, PbO powder (892.8 mg, 4mmol) was dissolved in a mixture of 57% w/w aqueous HI solution (4.0 mL, 30.4 mmol) and 50% aqueous H_3PO_2 (1mL, 9.1 mL) at room

temperature (25 °C) under constant magnetic stirring for 5 mins, which formed a bright yellow solution. Subsequent addition of solid CH_3NH_3Cl [135.2 mg, 2 mmol (n=2); 180 mg, 2.67 mmol (n=3); 202.8 mg, 3 mmol (n=4); 216 mg, 3.2 mmol (n=5)] at 230 °C initially caused the precipitation of black powders, which rapidly dissolved under stirring to afford a clear yellow solution. In a separate beaker, n-$CH_3(CH_2)NH_2$ [288 μL, 2.9 mmol (n=2); 170 μL, 1.71 mmol (n=3); 108.8 μL, 1.1 mmol (n=4); 88 μL, 0.89 mmol (n=5)] was neutralized with HI (2 mL, 15.2 mmol) in an ice bath resulting in a clear yellow solution. After adding the n-$CH_3(CH_2)_3NH_3I$ solution to the PbI_2 solution, the combined solution was kept at 230 °C, boiling for 10 mins. The solution was taken out and diluted 2 times with aqueous HI solution to afford a yellow clear solution, as the parent solution for the KCSC method.

2.1.3 Synthesis of (3AMP)$(MA)_2Pb_3I_{10}$ KCSC parent solution: DJ perovskites solution were synthesized by modifying the stoichiometry reported in the 3-(aminomethyl)pyridinium (3AMPY) 2D perovskites procedure.[37] The KCSC parent solution was diluted 3 times with aqueous HI solution and heated to 150 °C to ensure no crystals precipitated out before used to grow KCSC.

2.1.4 Growth of RP KCSC: Glass (quartz, sapphire could also be used) was used as the substrate for the 2D perovskite growth. Glass substrates were cut into 1-inch* 1-inch squares, cleaned in soap water, acetone, isopropanol by ultrasonication for 20 min each; then dried by argon. The substrates were transferred into a UV-Ozone cleaner, cleaned for 10 mins. The substrates were put on a hot plate, 10 μL of the parent solution was dropped onto the glass surface, another glass was put on top to fully cover the bottom glass and annealed. For n=1 large single crystal, n=1 parent solution is annealed at 70 °C for 6 hours. For n=2 large single crystal, n=2 parent solution is annealed at 70 °C for 6 hours. For n=3 large single crystal, n=3 parent solution is annealed at 60 °C for 5 hours. For n=4 large single crystal, n=3 parent solution is annealed at 80 °C for 6 hours. For n=5 large single crystal, n=3 parent solution is annealed at 95 °C for 4 hours. For n=6 large single crystal, n=4 parent solution is annealed at 105 °C for 10 hours. Then the top glass is removed, the crystal with the bottom glass is placed on spin coater, 40 μl *3 of the diethyl ether was dropped instantly and spin coated at 3000 r.p.m for 30 seconds followed by heating for 15 minutes to remove all the residue parent solution.

2.1.5 Growth of DJ KCSC: For DJ phase, a growth procedure similar to BA was used with adjustment of temperature and time. For n=3 large single crystal, n=3 parent solution is annealed at 60 °C for 6 hours. For n=4 large single crystal, n=3 parent solution is annealed at 80 °C for 5 hours. For n=5 large single crystal, n=3 parent solution is annealed at 96 °C for 6.5 hours. For n=6 large single crystal, n=4 parent solution is annealed at 105 °C for 10 hours.

2.2 X-ray diffraction measurements

The measurements were conducted using a Rigaku Smartlab X-Ray diffractometer with Cu(Kα) radiation (λ = 1.5406 Å). For each KCSC sample, it was measured right after removing the top glass and washing the crystal, with a step of 0.03^{o} and a speed of 3 degrees per minute. For the powder crystal, it dried in a vacuum oven at 65 °C overnight before measurement.

2.3 Grazing incidence wide angle x-ray scattering (GIWAXS)

The GIWAXS diffraction spectra used in this paper were high-resolution synchrotron patterns measured at 11-BM at the National Synchrotron Light Source-II (NSLS II). At beamline 11-BM, samples were placed on a robotic stage inside a vacuum chamber 6 (10-2 torr) with the sample 267mm away from a Pilatus 800K (Dectris) area detector. The photon energy was 13.5 keV, and the beam size was 200 μm × 50 μm (H × V).

2.4 In-situ absorbance measurements

The optical absorbance measurements were conducted using a broad-band light source (Thorlabs Solis-3C) focused onto the sample with a 50 μm beam size. The transmitted spectrum was collected by optical fiber and then sent to the spectrometer (Andor Kymera 328i) and CCD (Andor iDus 416). The measurement was conducted on the KCSC apparatus without removing the top glass.

2.5 In-situ PL imaging and spectrum measurements

The in-situ PL imaging was conducted based on a lab-built widefield microscope using a Mercury light source (Olympus U-LH100HG) for illumination source which was loosely focused onto the sample on the hot plate. The PL was spectrally filtered by a long-pass filter (BLP01-647R, Semrock) to selectively monitor the emission from RP BA n=4 crystal, and the PL images were monitored as time lapses recorded by a microscope camera (AmScope MU500). The in-situ PL

spectrum was collected on the same area by focusing a 543.5nm Helium-Neon Laser onto a 15 μm spot within the field of view of the PL image and was monitored by CCD spectrometer (Thorlabs CCS200). Both PL imaging and PL setup were interchangeable without repositioning the samples, allowing for spatially and spectrally-resolved in-situ PL tracing. Both measurements were conducted on the KCSC apparatus without removing the top glass.

References

(1) Stoumpos, C. C.; Cao, D. H.; Clark, D. J.; Young, J.; Rondinelli, J. M.; Jang, J. I.; Hupp, J. T.; Kanatzidis, M. G. Ruddlesden–Popper Hybrid Lead Iodide Perovskite 2D Homologous Semiconductors. *Chem. Mater.* **2016**, *28* (8), 2852–2867. https://doi.org/10.1021/acs.chemmater.6b00847.

(2) Mao, L.; Ke, W.; Pedesseau, L.; Wu, Y.; Katan, C.; Even, J.; Wasielewski, M. R.; Stoumpos, C. C.; Kanatzidis, M. G. Hybrid Dion–Jacobson 2D Lead Iodide Perovskites. *J. Am. Chem. Soc.* **2018**, *140* (10), 3775–3783. https://doi.org/10.1021/jacs.8b00542.

(3) Soe, C. M. M.; Stoumpos, C. C.; Kepenekian, M.; Traoré, B.; Tsai, H.; Nie, W.; Wang, B.; Katan, C.; Seshadri, R.; Mohite, A. D.; Even, J.; Marks, T. J.; Kanatzidis, M. G. New Type of 2D Perovskites with Alternating Cations in the Interlayer Space, $(C(NH_2)_3)(CH_3NH_3)_nPb_nI_{3n+1}$: Structure, Properties, and Photovoltaic Performance. *J. Am. Chem. Soc.* **2017**, *139* (45), 16297–16309. https://doi.org/10.1021/jacs.7b09096.

(4) Song, B.; Hou, J.; Wang, H.; Sidhik, S.; Miao, J.; Gu, H.; Zhang, H.; Liu, S.; Fakhraai, Z.; Even, J.; Blancon, J.-C.; Mohite, A. D.; Jariwala, D. Determination of Dielectric Functions and Exciton Oscillator Strength of Two-Dimensional Hybrid Perovskites. *ACS Mater. Lett.* **2021**, *3* (1), 148–159. https://doi.org/10.1021/acsmaterialslett.0c00505.

(5) Dou, L.; Wong, A. B.; Yu, Y.; Lai, M.; Kornienko, N.; Eaton, S. W.; Fu, A.; Bischak, C. G.; Ma, J.; Ding, T.; Ginsberg, N. S.; Wang, L.-W.; Alivisatos, A. P.; Yang, P. Atomically Thin Two-Dimensional Organic-Inorganic Hybrid Perovskites. *Science* **2015**, *349* (6255), 1518–1521. https://doi.org/10.1126/science.aac7660.

(6) Bao, Z.; Dodabalapur, A.; Lovinger, A. J. Soluble and Processable Regioregular Poly (3-hexylthiophene) for Thin Film Field-effect Transistor Applications with High Mobility. *Appl. Phys. Lett.* **1996**, *69* (26), 4108–4110.

(7) Mannsfeld, S. C.; Tee, B. C.; Stoltenberg, R. M.; Chen, C. V.; Barman, S.; Muir, B. V.; Sokolov, A. N.; Reese, C.; Bao, Z. Highly Sensitive Flexible Pressure Sensors with Microstructured Rubber Dielectric Layers. *Nat. Mater.* **2010**, *9* (10), 859–864.

(8) Kim, H.-S.; Lee, C.-R.; Im, J.-H.; Lee, K.-B.; Moehl, T.; Marchioro, A.; Moon, S.-J.; Humphry-Baker, R.; Yum, J.-H.; Moser, J. E. Lead Iodide Perovskite Sensitized All-Solid-State Submicron Thin Film Mesoscopic Solar Cell with Efficiency Exceeding 9%. *Sci. Rep.* **2012**, *2* (1), 1–7.

(9) Burschka, J.; Pellet, N.; Moon, S.-J.; Humphry-Baker, R.; Gao, P.; Nazeeruddin, M. K.; Grätzel, M. Sequential Deposition as a Route to High-Performance Perovskite-Sensitized Solar Cells. *Nature* **2013**, *499* (7458), 316–319.

(10) Blancon, J.-C.; Even, J.; Stoumpos, Costas. C.; Kanatzidis, Mercouri. G.; Mohite, A. D. Semiconductor Physics of Organic–Inorganic 2D Halide Perovskites. *Nat. Nanotechnol.* **2020**, *15* (12), 969–985. https://doi.org/10.1038/s41565-020-00811-1.

(11) Ghosh, D.; Acharya, D.; Pedesseau, L.; Katan, C.; Even, J.; Tretiak, S.; Neukirch, A. J. Charge Carrier Dynamics in Two-Dimensional Hybrid Perovskites: Dion–Jacobson *vs.* Ruddlesden–Popper Phases. *J. Mater. Chem. A* **2020**, *8* (42), 22009–22022. https://doi.org/10.1039/D0TA07205B.

(12) Milot, R. L.; Sutton, R. J.; Eperon, G. E.; Haghighirad, A. A.; Martinez Hardigree, J.; Miranda, L.; Snaith, H. J.; Johnston, M. B.; Herz, L. M. Charge-Carrier Dynamics in 2D Hybrid Metal–Halide Perovskites. *Nano Lett.* **2016**, *16* (11), 7001–7007. https://doi.org/10.1021/acs.nanolett.6b03114.
(13) Li, P.; Chen, Y.; Yang, T.; Wang, Z.; Lin, H.; Xu, Y.; Li, L.; Mu, H.; Shivananju, B. N.; Zhang, Y. Two-Dimensional CH3NH3PbI3 Perovskite Nanosheets for Ultrafast Pulsed Fiber Lasers. *ACS Appl. Mater. Interfaces* **2017**, *9* (14), 12759–12765.
(14) Xing, J.; Zhao, Y.; Askerka, M.; Quan, L. N.; Gong, X.; Zhao, W.; Zhao, J.; Tan, H.; Long, G.; Gao, L.; Yang, Z.; Voznyy, O.; Tang, J.; Lu, Z.-H.; Xiong, Q.; Sargent, E. H. Color-Stable Highly Luminescent Sky-Blue Perovskite Light-Emitting Diodes. *Nat. Commun.* **2018**, *9* (1), 3541. https://doi.org/10.1038/s41467-018-05909-8.
(15) Zhao, B.; Bai, S.; Kim, V.; Lamboll, R.; Shivanna, R.; Auras, F.; Richter, J. M.; Yang, L.; Dai, L.; Alsari, M.; She, X.-J.; Liang, L.; Zhang, J.; Lilliu, S.; Gao, P.; Snaith, H. J.; Wang, J.; Greenham, N. C.; Friend, R. H.; Di, D. High-Efficiency Perovskite–Polymer Bulk Heterostructure Light-Emitting Diodes. *Nat. Photonics* **2018**, *12* (12), 783–789. https://doi.org/10.1038/s41566-018-0283-4.
(16) Gong, X.; Voznyy, O.; Jain, A.; Liu, W.; Sabatini, R.; Piontkowski, Z.; Walters, G.; Bappi, G.; Nokhrin, S.; Bushuyev, O. Electron–Phonon Interaction in Efficient Perovskite Blue Emitters. *Nat. Mater.* **2018**, *17* (6), 550–556.
(17) Shi, C.; Ye, L.; Gong, Z.-X.; Ma, J.-J.; Wang, Q.-W.; Jiang, J.-Y.; Hua, M.-M.; Wang, C.-F.; Yu, H.; Zhang, Y.; Ye, H.-Y. Two-Dimensional Organic–Inorganic Hybrid Rare-Earth Double Perovskite Ferroelectrics. *J. Am. Chem. Soc.* **2020**, *142* (1), 545–551. https://doi.org/10.1021/jacs.9b11697.
(18) Liu, Y.; Han, S.; Wang, J.; Ma, Y.; Guo, W.; Huang, X.-Y.; Luo, J.-H.; Hong, M.; Sun, Z. Spacer Cation Alloying of a Homoconformational Carboxylate *Trans* Isomer to Boost in-Plane Ferroelectricity in a 2D Hybrid Perovskite. *J. Am. Chem. Soc.* **2021**, *143* (4), 2130–2137. https://doi.org/10.1021/jacs.0c12513.
(19) Zhai, Y.; Baniya, S.; Zhang, C.; Li, J.; Haney, P.; Sheng, C.-X.; Ehrenfreund, E.; Vardeny, Z. V. Giant Rashba Splitting in 2D Organic-Inorganic Halide Perovskites Measured by Transient Spectroscopies. *Sci. Adv.* **2017**, *3* (7), e1700704. https://doi.org/10.1126/sciadv.1700704.
(20) Huang, P.-J.; Taniguchi, K.; Miyasaka, H. Bulk Photovoltaic Effect in a Pair of Chiral–Polar Layered Perovskite-Type Lead Iodides Altered by Chirality of Organic Cations. *J. Am. Chem. Soc.* **2019**, *141* (37), 14520–14523.
(21) Fieramosca, A.; De Marco, L.; Passoni, M.; Polimeno, L.; Rizzo, A.; Rosa, B. L. T.; Cruciani, G.; Dominici, L.; De Giorgi, M.; Gigli, G.; Andreani, L. C.; Gerace, D.; Ballarini, D.; Sanvitto, D. Tunable Out-of-Plane Excitons in 2D Single-Crystal Perovskites. *ACS Photonics* **2018**, *5* (10), 4179–4185. https://doi.org/10.1021/acsphotonics.8b00984.
(22) Wang, J.; Li, J.; Lan, S.; Fang, C.; Shen, H.; Xiong, Q.; Li, D. Controllable Growth of Centimeter-Sized 2D Perovskite Heterostructures for Highly Narrow Dual-Band Photodetectors. *ACS Nano* **2019**, 12.
(23) Wang, K.; Wu, C.; Yang, D.; Jiang, Y.; Priya, S. Quasi-Two-Dimensional Halide Perovskite Single Crystal Photodetector. *ACS Nano* **2018**, *12* (5), 4919–4929. https://doi.org/10.1021/acsnano.8b01999.
(24) Soe, C. M. M.; Nagabhushana, G. P.; Shivaramaiah, R.; Tsai, H.; Nie, W.; Blancon, J.-C.; Melkonyan, F.; Cao, D. H.; Traoré, B.; Pedesseau, L.; Kepenekian, M.; Katan, C.; Even, J.; Marks, T. J.; Navrotsky, A.; Mohite, A. D.; Stoumpos, C. C.; Kanatzidis, M. G. Structural and Thermodynamic Limits of Layer Thickness in 2D Halide Perovskites. *Proc. Natl. Acad. Sci.* **2019**, *116* (1), 58–66. https://doi.org/10.1073/pnas.1811006115.
(25) Singh, A.; Lynch, J.; Anantharaman, S. B.; Hou, J.; Singh, S.; Kim, G.; Mohite, A. D.; Singh, R.; Jariwala, D. Cavity-Enhanced Raman Scattering from 2D Hybrid Perovskites. *J. Phys. Chem. C* **2022**, *126* (27), 11158–11164. https://doi.org/10.1021/acs.jpcc.2c01577.

(26) Anantharaman, S. B.; Stevens, C. E.; Lynch, J.; Song, B.; Hou, J.; Zhang, H.; Jo, K.; Kumar, P.; Blancon, J.-C.; Mohite, A. D.; Hendrickson, J. R.; Jariwala, D. Self-Hybridized Polaritonic Emission from Layered Perovskites. *Nano Lett.* **2021**, *21* (14), 6245–6252. https://doi.org/10.1021/acs.nanolett.1c02058.

(27) Li, W.; Sidhik, S.; Traore, B.; Asadpour, R.; Hou, J.; Zhang, H.; Fehr, A.; Essman, J.; Wang, Y.; Hoffman, J. M.; Spanopoulos, I.; Crochet, J. J.; Tsai, E.; Strzalka, J.; Katan, C.; Alam, M. A.; Kanatzidis, M. G.; Even, J.; Blancon, J.-C.; Mohite, A. D. Light-Activated Interlayer Contraction in Two-Dimensional Perovskites for High-Efficiency Solar Cells. *Nat. Nanotechnol.* **2021**. https://doi.org/10.1038/s41565-021-01010-2.

(28) Zhang, H.; Li, W.; Essman, J.; Quarti, C.; Metcalf, I.; Chiang, W.-Y.; Sidhik, S.; Hou, J.; Fehr, A.; Attar, A. Ultrafast Relaxation of Lattice Distortion in Two-Dimensional Perovskites. *Nat. Phys.* **2023**, 1–6.

(29) Li, J.; Wang, H.; Li, D. Self-Trapped Excitons in Two-Dimensional Perovskites. *Front. Optoelectron.* **2020**, *13*, 225–234.

(30) Blancon, J.-C.; Tsai, H.; Nie, W.; Stoumpos, C. C.; Pedesseau, L.; Katan, C.; Kepenekian, M.; Soe, C. M. M.; Appavoo, K.; Sfeir, M. Y.; Tretiak, S.; Ajayan, P. M.; Kanatzidis, M. G.; Even, J.; Crochet, J. J.; Mohite, A. D. Extremely Efficient Internal Exciton Dissociation through Edge States in Layered 2D Perovskites. *Science* **2017**, *355* (6331), 1288–1292. https://doi.org/10.1126/science.aal4211.

(31) Chen, Y.-X.; Ge, Q.-Q.; Shi, Y.; Liu, J.; Xue, D.-J.; Ma, J.-Y.; Ding, J.; Yan, H.-J.; Hu, J.-S.; Wan, L.-J. General Space-Confined On-Substrate Fabrication of Thickness-Adjustable Hybrid Perovskite Single-Crystalline Thin Films. *J. Am. Chem. Soc.* **2016**, *138* (50), 16196–16199. https://doi.org/10.1021/jacs.6b09388.

(32) Leng, K.; Abdelwahab, I.; Verzhbitskiy, I.; Telychko, M.; Chu, L.; Fu, W.; Chi, X.; Guo, N.; Chen, Z.; Chen, Z. Molecularly Thin Two-Dimensional Hybrid Perovskites with Tunable Optoelectronic Properties Due to Reversible Surface Relaxation. *Nat. Mater.* **2018**, *17* (10), 908–914.

(33) Sidhik, S.; Wang, Y.; De Siena, M.; Asadpour, R.; Torma, A. J.; Terlier, T.; Ho, K.; Li, W.; Puthirath, A. B.; Shuai, X. Deterministic Fabrication of 3D/2D Perovskite Bilayer Stacks for Durable and Efficient Solar Cells. *Science* **2022**, *377* (6613), 1425–1430.

(34) Stoumpos, C. C.; Soe, C. M. M.; Tsai, H.; Nie, W.; Blancon, J.-C.; Cao, D. H.; Liu, F.; Traoré, B.; Katan, C.; Even, J. High Members of the 2D Ruddlesden-Popper Halide Perovskites: Synthesis, Optical Properties, and Solar Cells of (CH3 (CH2) 3NH3) 2 (CH3NH3) 4Pb5I16. *Chem* **2017**, *2* (3), 427–440.

(35) Mao, L.; Kennard, R. M.; Traore, B.; Ke, W.; Katan, C.; Even, J.; Chabinyc, M. L.; Stoumpos, C. C.; Kanatzidis, M. G. Seven-Layered 2D Hybrid Lead Iodide Perovskites. *Chem* **2019**, *5* (10), 2593–2604. https://doi.org/10.1016/j.chempr.2019.07.024.

(36) Sidhik, S.; Li, W.; Samani, M. H. K.; Zhang, H.; Wang, Y.; Hoffman, J.; Fehr, A. K.; Wong, M. S.; Katan, C.; Even, J.; Marciel, A. B.; Kanatzidis, M. G.; Blancon, J.; Mohite, A. D. Memory Seeds Enable High Structural Phase Purity in 2D Perovskite Films for High-Efficiency Devices. *Adv. Mater.* **2021**, *33* (29), 2007176. https://doi.org/10.1002/adma.202007176.

(37) Li, X.; Ke, W.; Traoré, B.; Guo, P.; Hadar, I.; Kepenekian, M.; Even, J.; Katan, C.; Stoumpos, C. C.; Schaller, R. D.; Kanatzidis, M. G. Two-Dimensional Dion–Jacobson Hybrid Lead Iodide Perovskites with Aromatic Diammonium Cations. *J. Am. Chem. Soc.* **2019**, *141* (32), 12880–12890. https://doi.org/10.1021/jacs.9b06398.

(38) Fang, H.; Yang, J.; Tao, S.; Adjokatse, S.; Kamminga, M. E.; Ye, J.; Blake, G. R.; Even, J.; Loi, M. A. Unravelling Light-Induced Degradation of Layered Perovskite Crystals and Design of Efficient Encapsulation for Improved Photostability. *Adv. Funct. Mater.* **2018**, *28* (21), 1800305.

(39) Guo, Z.; Zhang, Y.; Wang, B.; Wang, L.; Zhou, N.; Qiu, Z.; Li, N.; Chen, Y.; Zhu, C.; Xie, H.; Song, T.; Song, L.; Xue, H.; Tao, S.; Chen, Q.; Xing, G.; Xiao, L.; Liu, Z.; Zhou, H. Promoting Energy Transfer via Manipulation of Crystallization Kinetics of Quasi-2D Perovskites for Efficient

Green Light-Emitting Diodes. *Adv. Mater.* **2021**, *33* (40), 2102246. https://doi.org/10.1002/adma.202102246.
(40) Li, X.; Hoffman, J. M.; Kanatzidis, M. G. The 2D Halide Perovskite Rulebook: How the Spacer Influences Everything from the Structure to Optoelectronic Device Efficiency. *Chem. Rev.* **2021**, *121* (4), 2230–2291. https://doi.org/10.1021/acs.chemrev.0c01006.
(41) Katan, C.; Mercier, N.; Even, J. Quantum and Dielectric Confinement Effects in Lower-Dimensional Hybrid Perovskite Semiconductors. *Chem. Rev.* **2019**, *119* (5), 3140–3192.
(42) Blancon, J.-C.; Stier, A. V.; Tsai, H.; Nie, W.; Stoumpos, C. C.; Traoré, B.; Pedesseau, L.; Kepenekian, M.; Katsutani, F.; Noe, G. T.; Kono, J.; Tretiak, S.; Crooker, S. A.; Katan, C.; Kanatzidis, M. G.; Crochet, J. J.; Even, J.; Mohite, A. D. Scaling Law for Excitons in 2D Perovskite Quantum Wells. *Nat. Commun.* **2018**, *9* (1), 2254. https://doi.org/10.1038/s41467-018-04659-x.

Acknowledgments: The work at Rice University was supported by start-up funds under the molecular nanotechnology initiative and also the DOE-EERE 2022-1652 program. J.H. acknowledges the financial support from the China Scholarships Council (No. 202107990007). W.L. acknowledges the National Science Foundation Graduate Research Fellowship Program (This material is based upon work supported by the National Science Foundation Graduate Research Fellowship Program under grant no. NSF 20-587. Any opinions, findings and conclusions or recommendations expressed in this material are those of the author and do not necessarily reflect the views of the National Science Foundation). Work at Northwestern on perovskite solar cells is supported by the Office of Naval Research Grant N00014-20-1-2725). D.J. acknowledges primary support for this work by the U.S. Army Research Office under contract number W911NF-19-1-0109 and the Sloan Fellowship in Chemistry awarded by the Alfred P. Sloan Foundation. S.B.A. gratefully acknowledges the funding received from the Swiss National Science Foundation (SNSF) under the Early Postdoc Mobility grant (P2ELP2_187977) for this work. J.E. acknowledges the financial support from the Institut Universitaire de France. The work at ISCR and Institut FOTON was performed with funding from the European Union's Horizon 2020 research and innovation program under grant agreement no. 861985 (PeroCUBE). This research used beamline 11-BM (CMS) of the NSLS-II and the Center for Functional Nanomaterials, both of which are US Department of Energy Office of Science User Facilities operated for the Department of Energy Office of Science by Brookhaven National Laboratory under contract no. DE-SC0012704. We thank Ruipeng Li and Esther Tsai for their assistance in performing experiments at beamline CMS. J.H. acknowledges the discussion with Prof. Ming Tang at Rice University and Prof. David Mitzi at Duke University.

Author contributions: J.H., J.-C.B. and A.D.M. conceived and designed the experiment. J.H. synthesized the perovskite single crystals with the help of S.S.. J.H. performed 1D-XRD measurements with the help of I.M., X.S. and A.M.. J.H. and H.Z. performed optical characterizations with the help of W.L. and S.B.A.. J.H. performed the transformation experiment. W.L. performed the machine learning analysis. J.H. performed data analysis with guidance from C.K., D.J., J.-C.B., M.K., J.E., and A. D. M.. J.H. and W.L. wrote the manuscript with input from everyone. All authors read the manuscript and agree to its contents, and all data are reported in the main text and supplemental materials.

Competing interests: The authors declare no competing interests.